Songklanakarin J. Sci. Technol.
41 (3), 669-678, May - Jun. 2019

http://www.sjst.psu.ac.th

Original Article

Shear strengths of fractures in Tak granite under orthotropic stresses

Pajeeraporn Weingchanda, Supattra Khamrat, Thanitta Thongprapa, and Kittitep Fuenkajorn*

Geomechanics Research Unit, Institute of Engineering,
Suranaree University of Technology, Mueang, Nakhon Ratchasima, 30000 Thailand

Received: 25 December 2017; Revised: 9 February 2018; Accepted: 17 February 2018

Abstract

The objective of this study is to determine the shearing resistance of fractures in Tak granite as affected by orthotropic stress states where $\sigma_1 \neq \sigma_2 \neq \sigma_3$. Triaxial shear tests are performed to obtain the strengths and dilations of tension-induced fractures and smooth saw-cut surfaces under confining pressures up to 18 MPa. The ratios of the lateral stresses vary from 0 to 4. The shearing resistance, dilation and areas of sheared-off asperities of the rough fractures decrease when the lateral stress ratios increase. The shear strengths of smooth saw-cut surfaces tend to be independent of the stress ratios. The distortional strain energy (W_d) required to displace the fractures under various stress states increases linearly with the mean strain energy (W_m). The energy ratio (W_d/W_m) in terms of the strains and dilation can be used as a predictive tool for the movements of faults or fractures in Tak granite.

Keywords: dilation, strain energy, orthotropic stress, fault

1. Introduction

Frictional behavior of rock fractures has normally been determined by the direct shear test method (ASTM D5607-08). The results have been applied to determine the stability of rock slope embankments, shallows rock foundations and underground openings. The test configurations however have some disadvantages. The magnitudes of the applied normal stress are limited by the uniaxial compressive strength of the rock, and the fractures are sheared under unconfined conditions. The results can not describe the friction behavior and movement of the fractures or faults at great depth where they are under high confinements. The triaxial shear test method (Barton, 1976; Brady & Brown, 2006; Jaeger *et al.*, 2007; Li *et al.*, 2012a, 2012b) has therefore been developed to simulate the frictional resistance of rock fractures under confining pressures. The normal stress at which the shear strengths are measured can be controlled by the applied axial stress and confining pressures (Lane & Heck, 1964; Rosso, 1976). The test provides the shear strengths of rock fractures under uniform lateral confining stresses ($\sigma_1 \neq \sigma_2 = \sigma_3$), which may also not truly represent their actual in-situ conditions, where $\sigma_1 \neq \sigma_2 \neq \sigma_3$. It has long been recognized that the intermediate principal stress or the true triaxial stress condition can notably affect the intact rock strengths and deformability (Alexeev *et al.*, 2008; Cai, 2008; Colmenares & Zoback, 2002; Haimson, 2006; Haimson & Chang, 2000; Haimson & Rudnicki, 2010). Rare attempt has however been made at determining the shear strengths of rock fractures under true triaxial stress states (Kapang *et al.*, 2013; Morris & Ferrill, 2009). A shear strength criterion for rock fractures that can incorporate the effect of the three-dimensional stresses has never been developed. Such knowledge could improve an understanding of the friction of rock fractures around deep underground structures and of the fault movements at great depth.

The objective of this study is to determine the shearing resistance of fractures in Tak granite as affected by orthotropic stresses when the three principal stresses are unequal. True triaxial shear tests are performed on tension-induced fractures and smooth saw-cut surfaces in Tak granite specimens. A polyaxial load frame is used to obtain the strengths and dilations of the fractures under confining pres-

*Corresponding author
Email address: kittitep@sut.ac.th

sures from 1 to 18 MPa. The lateral stress ratios are also varied from 0 to 4. The joint roughness coefficients (JRC) are determined prior to and after shearing. The strain energy principle is applied to describe the peak shear strengths and confinements under varied stress conditions.

2. Sample Preparation

The specimens used for the triaxial shear tests are prepared from the Tak granite. The granite batholith is ex-posed in the northwest of Thailand where there are several active faults and seismic activities (Fenton *et al.*, 2003). The tested granite is felsic phaneritic, and fine grained with average sizes of 4-5 mm. It comprises 40% plagioclase (with grain sizes of 0.5-1 mm), 30% quartz (2-5 mm), 5% ortho-clase (3-5 mm), 3% amphibole (1-2 mm), and 2% biotite (1-2 mm) (Kemthong & Fuenkajorn, 2007). The average density of the specimens is 2.67 g/cc. Rodklang *et al*. (2015) determine the mechanical properties of the Tak granite as: uniaxial compressive strength = 118 ± 5.2 MPa, elastic modulus = 13.8 GPa, Poisson's ratio = 0.28, cohesion = 17.6 MPa, and inter-nal friction angle = 58°. The specimens are cut to obtain rec-tangular blocks with nominal dimensions of 50×50×87 mm^3. The fractures are artificially made to obtain tension-inducing fracture and saw-cut surface. A line load is applied to obtain a tension-induced fracture diagonally across the rock block. The fracture area is 50×100 mm^2. The normal to the fracture plane makes an angle (β) of 59.1° with the major axis of the speci-men. The fractures are clean and well mated. The asperity amplitudes are measured from the laser-scanned profiles along the shearing direction. The readings are made to the nearest 0.01 mm. The maximum amplitudes of the profiles are used to determine the joint roughness coefficients (JRC) of each frac-ture based on the Barton's chart (Barton, 1982). The joint roughness coefficients are averaged as 12±1.0. All fractures show both first and second order asperities.

3. Test Apparatus and Method

A polyaxial load frame (Fuenkajorn *et al.*, 2012; Fuenkajorn & Kenkhunthod, 2010) is used to apply true tria-xial stresses to the specimens (Figure 1). One of the lateral stresses is parallel to the strike of the fracture plane and is designated as σ_p. The other is normal to the fracture strike and is designated as σ_o. They are applied by two pairs of 152 cm long cantilever beams set in mutually perpendicular directions of the polyaxial load frame. The axial stress representing the major principal stress (σ_1) is applied by a 1000-kN hydraulic load cell connected to an electric oil pump via a pressure regulator. Neoprene sheets are placed at all interfaces between loading platens and rock surfaces to minimize the friction. The specimen deformations in the three loading directions are monitored. The reading are recorded every 10 kN of the axial load increment. The frictional resistance at the interfaces between the loading platens and the lateral neoprene sheets are determined by vertically loading an intact specimen with the same dimensions while the constant lateral stresses paral-lel to the fracture are applied. The vertical stress induced by friction will be used to correct the axial loads during fracture shearing. The lateral stress ratios are varied (σ_p/σ_o) from 0, 1, 1.5, 2, 2.5, 3 to 4, when σ_o varies from 1 to 18 MPa. The block specimen with the fracture is first subjected to a pre-defined initial stress where σ_1 is first set equal to the lateral stress normal to the fracture plane (σ_3). The axial stress is then increased under a constant rate of 0.01 mm/s while σ_p and σ_o are maintained constant.

The shear stress (τ) and its corresponding normal stress (σ_n) can be determined as follows (Jaeger *et al.*, 2007):

$$\tau = 1/2(\sigma_1-\sigma_o)^2 \cdot \sin 2\beta \quad (1)$$

$$\sigma_n = 1/2\,(\sigma_1+\sigma_o) + 1/2(\sigma_1-\sigma_o) \cdot \cos 2\beta \quad (2)$$

where σ_1 and σ_o are the axial and lateral stresses and β is the angle between σ_1 and σ_n directions. For all specimens the angle β equals to 59.1°.

The shear and normal (dilation) displacement (d_s and d_n) can be calculated from the measured vertical and lateral displacements (d_1 and d_3) as follows (Kleepmek *et al.*, 2016):

$$d_s = d_1/\sin\beta \quad (3)$$

$$d_n = (d_{3,m}-d_{3,c}) \cdot \sin\beta \quad (4)$$

$$d_{3,c} = d_1 \cdot \tan(90-\beta) \quad (5)$$

where $d_{3,m}$ is the total lateral displacement measured during the test, and $d_{3,c}$ are the calculated lateral displacement induced by the vertical displacement on the incline fracture plane.

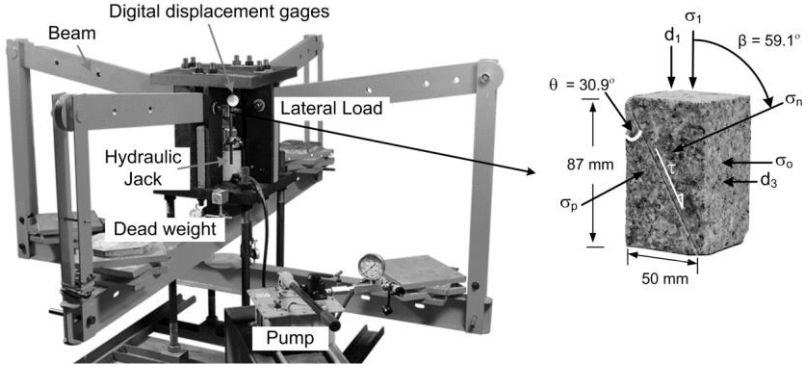

Figure 1. Polyaxial load frame used in this study (Fuenkajorn & Kenkhunthod, 2010; Fuenkajorn *et al.*, 2012).

4. Test Results

Figure 2 shows the major principal stresses (σ_1) as a function of vertical displacements (d_1), and lateral displacements (d_o) as a function of vertical displacements (d_1) for the tension-induced fractures. The diagrams show that the larger lateral stress ratios induce lower peak and residual stresses. The stress ratios also decrease the fracture dilation at the peak stress. The axial stresses corresponding to the peak shear strengths are plotted as a function of the lateral stress,σ_o, for various σ_p/σ_o ratios in Figure 3a, showing that the stress ratios can significantly reduce the fracture shear strengths for all σ_o values. To incorporate all principal stresses applied on the fractures the octahedral shear strengths (τ_{oct}) at the peak point are derived and presented as a function of the mean stress as shown in Figure 3b. The effect of the stress ratios is enhanced when the mean stress increases. This suggests that the stress ratio effect becomes even more significant under greater depth. Table 1 summarizes the shear strength results and their corresponding normal stress for different σ_p/σ_o ratios.

The shear strength of the smooth saw-cut surfaces tends to be independent of the lateral stress ratio, as shown in the $\sigma_{1,p}$-σ_o and τ_{oct} -σ_m diagrams in Figure 3. Note that as the stress ratio increases the τ_{oct}/σ_m slopes of the tension-induced fractures approach those of the smooth saw cut surface. This suggests that fractures under high lateral stress ratio (σ_p/σ_o) can displace more smoothly and easily than those under lower stress ratio, and that under higher stress ratios, the fracture roughness becomes less significant.

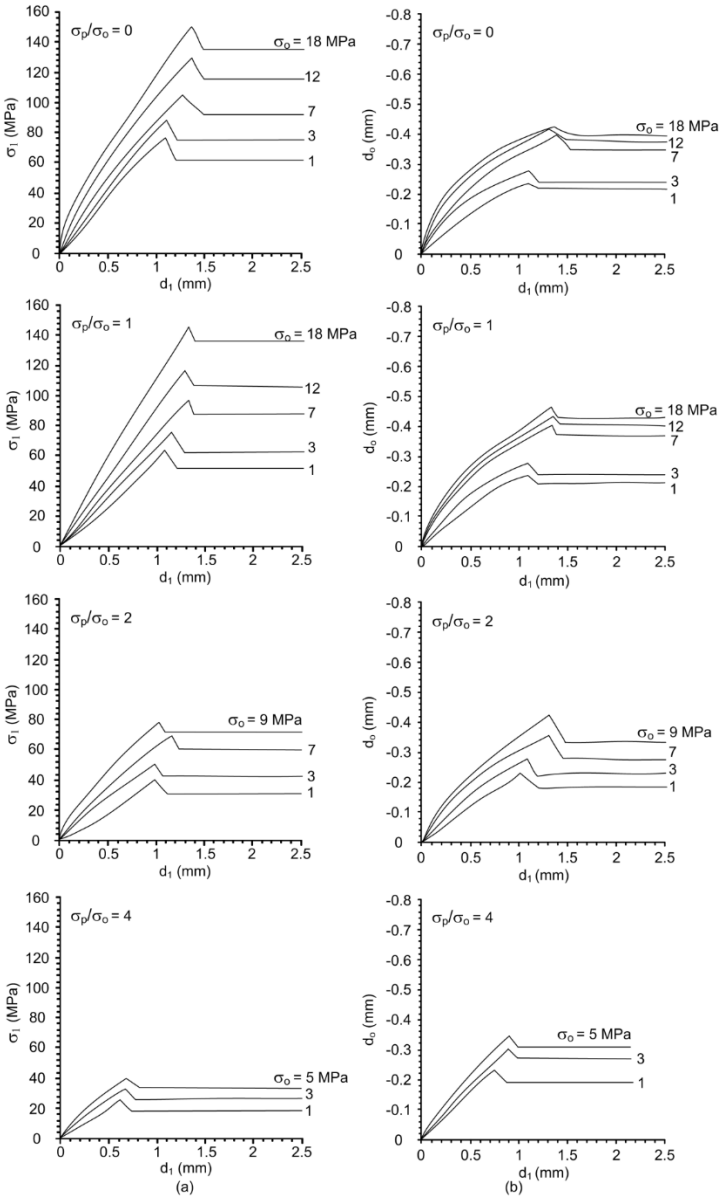

Figure 2. Major principal stresses as a function of vertical displacements (a), and lateral displacements as a function of vertical displacements (b).

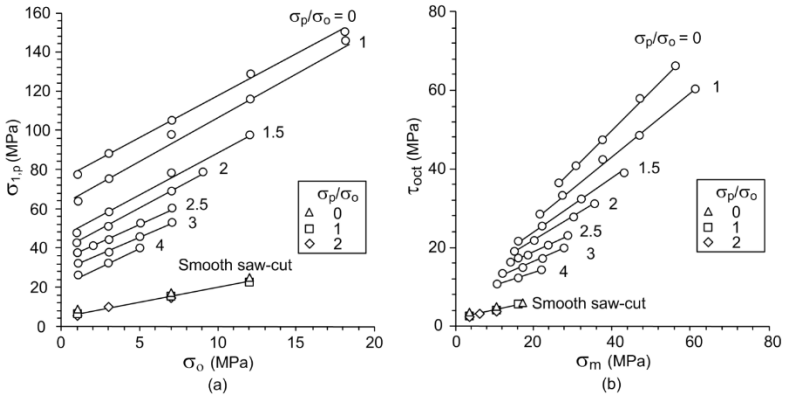

Figure 3. Major principal stresses at peak ($\sigma_{1,p}$) as a function confining stresses (σ_o) (a), and octahedral shear stresses as a function of mean stress (b) .

Table 1. Peak shear strengths and their corresponding normal stresses for different σ_p/σ_o ratios.

Fracture Types	σ_p/σ_o	JRC	σ_p (MPa)	σ_o (MPa)	$\sigma_{1,p}$ (MPa)	τ_p (MPa)	σ_n (MPa)	τ_{oct} (MPa)	γ_{oct} ($\times 10^{-3}$)
Tension-Induced Fracture	0	13	0	1	77.72	33.15	20.14	36.40	7.93
		13	0	3	88.40	36.43	25.19	40.98	8.09
		11	0	7	105.45	42.63	31.61	48.14	8.85
		10	0	12	129.46	50.77	41.31	58.41	9.01
		11	0	18	150.65	57.56	51.21	67.18	9.34
	1	13	1	1	63.22	26.98	16.58	29.33	8.24
		11	3	3	75.30	29.31	21.07	34.08	8.81
		10	7	7	98.20	35.49	29.80	42.99	9.44
		10	12	12	116.59	44.20	39.83	49.30	10.33
		11	18	18	146.50	49.64	50.12	60.58	10.50
	1.5	13	1.5	1	48.22	20.48	12.80	22.14	8.58
		13	4.5	3	58.80	24.03	16.95	25.96	9.21
		11	10.5	7	78.51	30.24	24.72	32.92	9.92
		10	18	12	98.28	37.00	33.57	39.33	10.71
	2	13	2	1	41.18	18.45	11.65	18.71	8.80
		11	6	3	50.90	20.81	14.98	21.91	9.22
		11	14	7	69.38	26.12	22.34	27.90	10.31
		13	18	9	79.84	30.15	27.83	31.49	10.94
	2.5	13	2.5	1	38.07	16.07	10.28	17.13	8.86
		13	5	2	40.95	16.88	11.75	17.70	9.12
		11	7.5	3	44.41	17.91	13.34	18.55	9.65
		11	12.5	5	52.59	20.68	16.94	20.89	10.09
		11	17.5	7	60.87	23.22	20.41	23.32	10.44
	3	11	3	1	32.00	13.23	8.60	14.17	9.04
		13	9	3	38.22	15.80	12.12	15.38	9.75
		11	15	5	45.80	17.69	15.22	17.36	10.23
		13	21	7	52.62	19.74	18.40	19.08	10.58
	4	10	4	1	26.23	10.84	7.26	11.25	9.29
		11	12	3	32.45	12.89	10.44	12.32	9.87
		10	20	5	40.18	15.37	13.87	14.41	10.57
Smooth saw-cut surface	0	-	0	1	7.89	2.98	2.72	3.25	5.64
		-	0	7	16.83	4.26	9.46	4.63	6.94
		-	0	12	24.65	5.48	15.16	5.96	8.46
	1	-	1	1	7.48	2.81	2.62	3.05	9.23
		-	7	7	16.32	4.04	9.33	4.39	9.17
		-	12	12	23.80	5.11	14.95	5.56	11.09
	2	-	2	1	6.97	2.59	2.49	2.81	7.68
		-	6	7	10.71	3.34	4.93	3.63	8.09
		-	14	12	16.15	3.96	9.29	4.31	10.08

5. Fracture Dilation

The shear and normal (dilation) displacements (d_s and d_n) of the fractures can be calculated using Equations 3 and 4. Under the some σ_o, the fractures dilation at the peak strength decreases with increasing lateral stress ratios, as shown in Figure 4a, suggesting that the fracture asperities tend to be sheared-off more under large lateral stress ratio than those under lower stress ratio. Figure 4a also shows that the stress ratio can reduce the dilation rate more effective than the confining stress, σ_o, can. This agrees with the experimental results obtained by Kapang *et al.* (2013) on fractures in sandstone. This is probably because the stress that is parallel to the fracture plane can cause localized stress concentration at the fracture asperities, and hence reduces the fracture shear strength. This is supported by the JRC measurements obtained after shearing, as shown in Figure 4b. The smoother sheared fracture surfaces (lower JRC's) are obtained under higher lateral stress ratios. Examples of the laser-scanned images obtained before and after shearing are given in Figure 5, which confirms the visual observations of the post-test fractures that the sheared-off areas increase with the lateral stress ratio.

6. Empirical Criterion

An attempt is made here to develop an empirical strength criterion that can explicitly incorporate the effect of the lateral stress ratio and the normal stress. The power equation is proposed as follows:

$$\tau = \delta \cdot \sigma_n^{\omega} \tag{6}$$

where δ and ω are empirical constants. The above equation is fitted to the experimental results in the forms of τ-σ_n diagrams in Figure 6. Non-linear behavior of the τ-σ_n relation is observed. Regression analysis of the test data by SPSS software (Colin & Paul, 2012) are performed on Equation 6 using the peak shear strength data given in Table 1. The parameter ω can be defined as 0.566 and 0.334 for rough and smooth surfaces. The parameter δ decreases with increasing the stress ratios (σ_p /σ_o), which can be described by a linear equation:

$$\delta = \psi - \eta \cdot (\sigma_p / \sigma_o) \tag{7}$$

where ψ and η are empirical constants. For the tension-induced

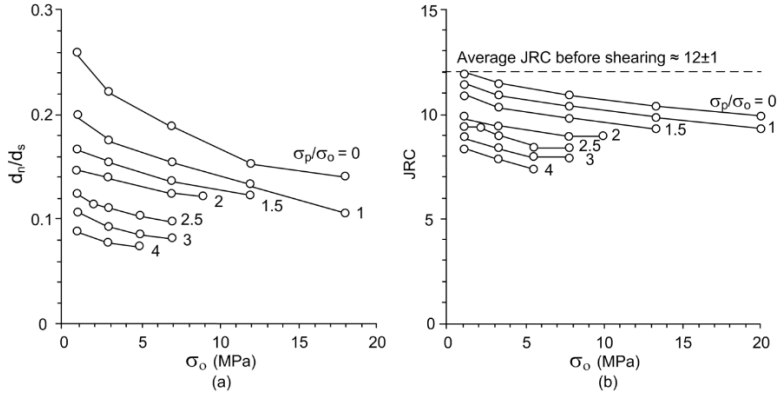

Figure 4. Dilation rates (d_n/d_s) as a function of confining stresses (σ_o) (a) and post-test JRC's as a function of σ_o (b).

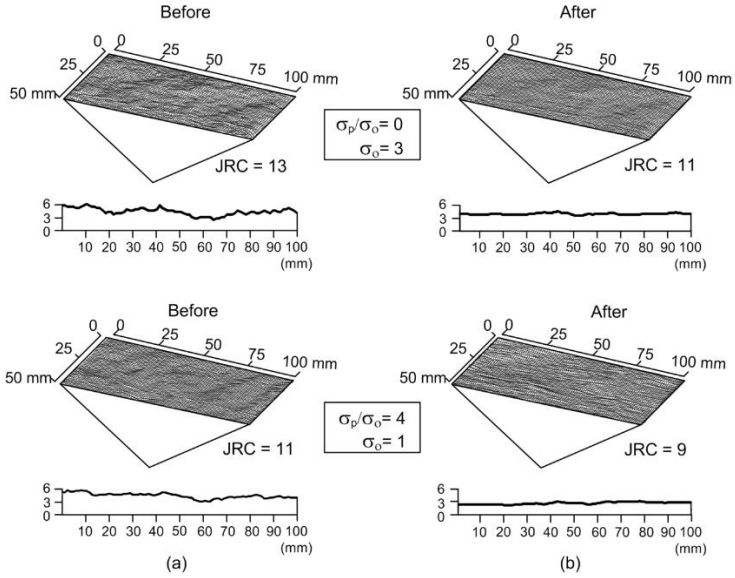

Figure 5. Three-dimensional laser scanning images of fractures before (a) and after (b) shearing.

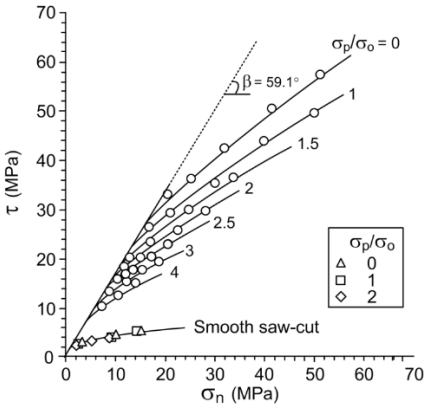

Tension-induced

σ_p/σ_o	$\tau = \delta\sigma_n^{\omega}$		R^2
	δ	ω	
0	5.231	0.609	0.995
1	5.236	0.573	0.989
1.5	4.262	0.613	0.999
2	4.571	0.564	0.997
2.5	4.424	0.546	0.992
3	4.295	0.522	0.999
4	3.717	0.536	0.994
$\omega^*_{Average}$=0.566			

Smooth saw-cut

σ_p/σ_o	$\tau = \delta\sigma_n^{\omega}$		R^2
	δ	ω	
0	2.091	0.340	0.976
1	2.013	0.332	0.982
2	1.942	0.329	0.991
$\omega^*_{Average}$=0.334			

Figure 6. Shear strengths (τ) as a function of normal stress (σ_n) for tension-induced fracture and smooth saw-cut surfaces.

(rough) fractures the parameters ψ and η are 5.274 and 0.370. For the saw-cut (smooth) fractures ψ and η are 2.090 and 0.075. Equations 6 and 7 fit well with the test results (R^2>0.9).

7. Strain Energy Density Criterion under Lateral Stress Ratios

The activation energy has been widely used for the predictions of fault movements under great depth (high confining pressures) and elevated temperatures (Odedra *et al.*, 2001; Ohnaka, 1995; Stesky, 1978), where the fault dilation is neglected (i.e. plastic deformation of the shear zone). For shallow faults or fractures with low temperatures the lateral dilation of the fractures (brittle deformation) can not be ignored. An alternative approach is used here. The strain energy density principle is applied to describe the fracture strength and deformation under high confining pressures. The distor-tional strain energy (W_d) required to displace the fractures can be defined as a function of mean strain energy (W_m) as follows:

$$W_d = \delta \cdot W_m \quad (8)$$

where δ is an empirical constant. The distortional and mean strain energies can be calculated from the test results as (Jaeger *et al.,* 2007):

$$W_d = 3/2\ \tau_{oct} \cdot \gamma_{oct} \quad (9)$$
$$W_m = 3/2\ \sigma_m \cdot \varepsilon_m \quad (10)$$

where τ_{oct} and γ_{oct} are octahedral shear stress and strain, and σ_m and ε_m are mean stress and mean strain. For the test conditions used here, the strain along the fracture strike is equal to zero (ε_p= 0). As a result the shear and mean stress and strain at the peak point can be determined as:

$$\gamma_{oct} = (1/3)\ [2\ (\varepsilon_{1,p} - \varepsilon_{o,p})^2]^{1/2} \quad (11)$$
$$\tau_{oct} = (1/3)\ [(\sigma_{1,p} - \sigma_{p,p}) + (\sigma_{1,p} - \sigma_{o,p})]^{1/2} \quad (12)$$
$$\sigma_m = (\sigma_{1,p} + \sigma_{p,p} + \sigma_{o,p}) / 3 \quad (13)$$
$$\varepsilon_m = (\varepsilon_{1,p} + \varepsilon_{o,p}) / 3 \quad (14)$$

where $\sigma_{1,p}$, $\sigma_{p,p}$ and $\sigma_{o,p}$ are the stresses at the peak point, and $\varepsilon_{1,p}$ and $\varepsilon_{o,p}$ are the strains at the peak point. Assuming that the intact portion of the specimen is rigid, the vertical and lateral strains can be determined from the fracture displacements:

$$\varepsilon_{1,p} = d_{1,p} / L \quad (15)$$
$$\varepsilon_{o,p} = d_{o,p} / W \quad (16)$$

where $d_{1,p}$ and $d_{o,p}$ are the vertical displacement and lateral displacement normal to the fracture strike, L is the specimen length (87 mm), and W is the specimen width (50 mm). Table 2 gives the distortional and mean strain energy calculated for the rough and smooth fractures. Note that the strain that is parallel to the fracture strike is equal to zero because the test configurations (loading platens) do not allow lateral displacement in this direction.

Regression analysis of Equations 8 indicates that δ equals to 4.78 for the rough fractures, and equals to 1.42 for the smooth fractures (Figure 7). The proposed criterion fit well to the test data with the correlation coefficient (R^2) greater than 0.9. It implicitly incorporates the effects of stress ratio and confining pressure on the fractures. The W_d obtained from the rough fractures under high stress ratio is in the lower portion of the curve. The mean strain energy can be related to the depth of the fractures. The distortional strain energy represents the deviatoric stresses that cause the shear displacement. The ratio of W_d to W_m (or δ) is probably governed by the roughness and strength of the fracture asperities. The W_d-W_m curve of the smooth fractures would represent the lower bound of the energy required to shear the fractures.

From Equations 9 and 10 the W_d and W_m can be written as (Jaeger *et al.,* 2007):

$$W_d = 3G \cdot \gamma_{oct}^2 \quad (17)$$
$$W_m = (9/2)\ K \cdot \varepsilon_m^2 \quad (18)$$

where G and K are the shear and bulk modulus:

$$G = E / [2(1+\nu)] \quad (19)$$
$$K = E / [3(1-2\nu)] \quad (20)$$

where E is the elastic modulus, and ν is the Poisson's ratio. The slope of the W_d-W_m curve can be represented by:

$$W_d / W_m = (\gamma_{oct} / \varepsilon_m)^2\ [(1-2\nu) / (1+\nu)] \quad (21)$$

Table 2. Distortional and mean strain energy densities for different σ_p/σ_o ratios.

Fracture Types	σ_p/σ_o	σ_p (MPa)	σ_o (MPa)	$d_{1,p}$ (mm)	$d_{o,p}$ (mm)	$\varepsilon_{1,p}$ (milli-strain)	$\varepsilon_{o,p}$ (milli-strain)	W_d (kPa)	W_m (kPa)
Tension-Induced Fracture	0	0	1	1.09	-0.33	12.53	-6.58	405.53	78.05
		0	3	1.11	-0.34	12.76	-6.74	470.88	91.68
		0	7	1.20	-0.38	13.79	-7.58	613.22	116.44
		0	12	1.22	-0.39	14.02	-7.76	767.65	147.66
		0	18	1.26	-0.41	14.48	-8.10	925.54	179.41
	1	1	1	1.11	-0.36	12.76	-7.16	338.86	60.86
		3	3	1.18	-0.39	13.54	-7.78	420.07	78.05
		7	7	1.25	-0.43	14.37	-8.50	565.98	109.73
		12	12	1.35	-0.48	15.52	-9.56	707.63	139.59
		18	18	1.37	-0.49	15.75	-9.74	883.10	182.72
	1.5	1.5	1	1.13	-0.39	12.99	-7.82	263.17	43.69
		4.5	3	1.20	-0.43	13.79	-8.56	327.12	57.83
		10.5	7	1.28	-0.47	14.71	-9.38	439.86	85.33
		18	12	1.37	-0.52	15.75	-10.30	559.21	116.46
	2	2	1	1.15	-0.41	13.23	-8.12	235.62	37.63
		6	3	1.20	-0.43	13.79	-8.60	301.78	51.84
		14	7	1.32	-0.49	15.17	-9.90	453.05	79.42
		18	9	1.39	-0.53	16.02	-10.60	551.19	96.57
	2.5	2.5	1	1.15	-0.42	13.22	-8.30	218.35	34.08
		5	2	1.18	-0.43	13.56	-8.60	239.69	39.66
		7.5	3	1.24	-0.46	14.25	-9.20	272.76	46.24
		12.5	5	1.29	-0.49	14.83	-9.70	334.25	59.90
		17.5	7	1.33	-0.51	15.29	-10.10	397.50	73.81
	3	3	1	1.16	-0.43	13.38	-8.58	186.06	28.80
		9	3	1.25	-0.47	14.31	-9.40	234.82	41.10
		15	5	1.30	-0.49	14.94	-9.94	291.48	54.86
		21	7	1.34	-0.52	15.40	-10.36	343.35	67.75
	4	4	1	1.19	-0.45	13.68	-8.92	155.42	24.77
		12	3	1.26	-0.48	14.43	-9.60	198.30	38.16
		20	5	1.34	-0.52	15.34	-10.40	258.68	53.72
Smooth saw-cut surface	0	0	1	1.00	-0.05	11.49	-0.90	27.42	17.50
		0	7	1.02	-0.24	11.72	-4.80	46.28	35.58
		0	12	1.15	-0.36	13.22	-7.20	70.92	48.80
	1	1	1	1.27	-0.13	18.14	-2.60	42.00	24.56
		7	7	1.29	-0.36	14.83	-7.20	57.25	38.54
		12	12	1.37	-0.51	16.71	-10.20	85.78	51.84
	2	2	1	1.28	-0.14	14.71	-2.80	32.06	17.81
		6	3	1.30	-0.19	14.94	-3.80	43.29	31.03
		14	7	1.44	-0.38	16.55	-7.60	62.07	44.98

Equations 17 through 21 are based on the linear elastic theory. From the assumption posed in the previous section that the intact portion of the specimen is rigid. All deformations measured during shearing can be taken as the axial displacement (d_1) and the lateral displacement (d_o) of the fractures. The $-d_o/d_1$ is defined here as the lateral displacement rate. The energy ratio (W_d/W_m) of the tested specimens can therefore be approximated from the $-d_o/d_1$ as:

$$W_d / W_m = (\gamma_{oct} / \varepsilon_m)^2 [(1+2\, d_o/d_1) / (1- d_o/d_1)] \qquad (22)$$

The $(\gamma_{oct} / \varepsilon_m)^2$ function relates to the induced strains required to reach the peak strength of the fractures. The $[(1+2\, d_o/d_1) / (1- d_o/d_1)]$ function, called here as displacement function, relates to the fracture displacements. The octahedral shear strain-to-mean strain ratio is plotted as a function of the mean stress for all stress ratios in Figure 8a. The ratios increase with the mean stress (or depth). A higher stress ratio leads to a more plastic deformation of the fractures or less brittle movement. The displacement functions are plotted as a function of mean stress in Figure 8b. The diagram suggests that the functions decrease when the confining pressures and the stress ratios increase.

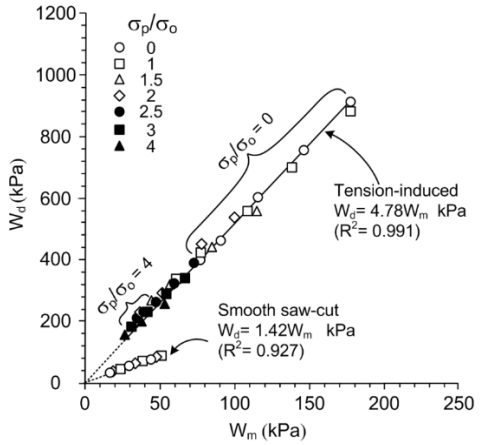

Figure 7. Distortional strain energy (W_d) at peak shears strength as a function of mean strain energy (W_m).

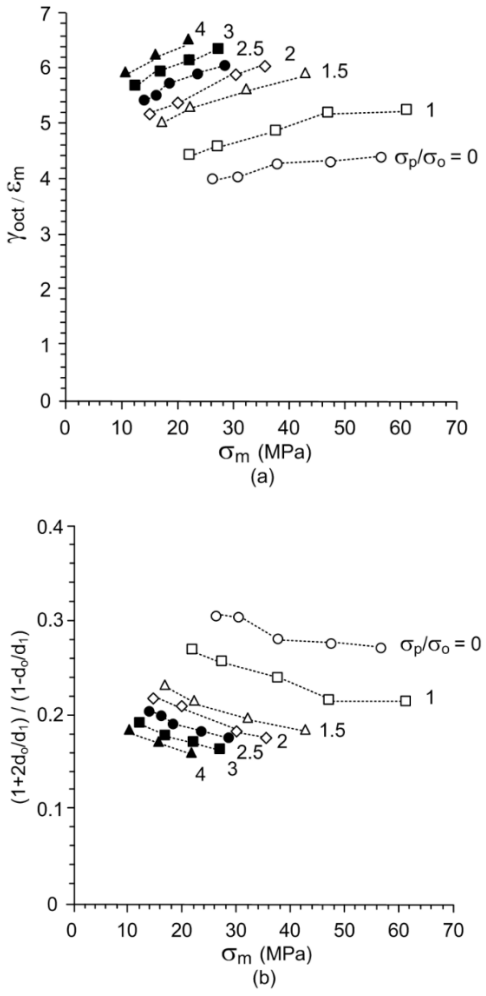

Figure 8. Octahedral shear strain-to-mean strain ratio as a function of mean stress (a), and displacement function as a function of mean stress (b).

8. Discussion and Conclusions

Triaxial shear tests have been performed on rough (tension-induced) and smooth (saw-cut) fractures in Tak granite under confining pressures between 1 and 18 MPa with varying lateral stress ratios from 0 to 4. The results indicate that the rough fracture shear strengths decrease when the stress ratios increase. The areas of the sheared-off asperities increase with the confining pressure, as evidenced by the lower JRC values measured from the post-test fractures. This results in the lower dilation rates at the peak strength (Figure 4). The effects of the stress ratio and confining pressure on the shear strengths of the rough fractures can be well described by a power equation (Equation 6). The equation can be used as a strength criterion to determine the stability of engineering structures near ground surface (e.g., foundations, slope embankments and tunnels) where the applied shear and normal stresses and stress ratio are known. It may not be appropriate for use as a predictive tool for the fault movements where the needed stress components can not be monitored accurately at depths.

An attempt has been made at deriving a criterion that can be used to predict a shallow fault movement in the Tak granite batholith. The distortional and mean strain energy densities are calculated from the test results. Their linear relation has implicitly incorporated the effects of lateral stress ratio and confining pressure (Figure 7). The slope (δ) of the W_d-W_m ratio is dependent of the fracture roughness and strength of the asperities. Assuming that the rock adjacent to a fault is a rigid body, and that all deformations are from the shear and dilation within the fault. The energy ratio can be derived here in terms of the shear strain-to-mean strain ratio and the displacement function. The strain ratios increase with confining pressure and stress ratio. The displacement functions decrease as the pressure and lateral stress ratio increase. Their components can be obtained from the on- or near- surface measurements. This may allow estimating the strength of the shallow faults in the Tak batholith by calculating the changes of the energy ratios (or δ) from the displacements monitored along the fault line. In principle the measured energy ratios along a fault line would slowly increase with time due to the tectonic forces. The earthquake or seismic events will occur when the energy ratio (δ) reaches the criterion defined in Figure 7.

It is recognized that there are other factors governing the fault strengths that are not studied here, for example pore pressures, displacement rates, temperature and fracture/fault roughness (Barton & Choubey, 1977; Belem *et al.,* 2000; Blacic, 1975; Crawford & Currant, 1981; Curran & Leong, 1983; Yeo *et al.,* 1998). The effects of these factors may alter the accuracy of the proposed equation, but they would not change the main conclusions drawn here. The proposed strain energy concept nevertheless is a precursory step toward the prediction of the seismic activities caused by the movement of shallow fault zones.

Acknowledgements

This research is funded by Suranaree University of Technology and by the Higher Education Promotion and National Research University of Thailand. Permission to publish this paper is gratefully acknowledged.

References

Alexeev, A. D., Revva, V. N., Bachurin, L. L., & Prokhorov, I. Y. (2008). The effect of stress state factor on fracture of sandstones under true triaxial loading. *International Journal of Fracture*, *149*(1), 1-10. doi:10.1007/s10704-008-9214-6

ASTM D5607-08. Standard Test Method for Performing Laboratory Direct Shear Strength Tests of Rock Specimens Under Constant Normal Force. Annual Book of ASTM Standards, Philadelphia: American Society for Testing and Materials, Vol. 04.08, West Conshohocken, P.A: ASTM.

Barton, N. (1976). The Shear strength of rock and rock joint. *International Journal of Rock Mechanics and Mining Science and Geomechanics Abstracts*, *13*(9), 255-279. doi:10.1016/0148-9062(76)90003-6

Barton, N. (1982). Characterizing rock masses to improve excavation design. *Proceeding of 4th Congress international Association for Engineering Geology and Environment*, New Delhi.

Barton, N., & Choubey, V. (1977). The shear strength of rock joints in theory and practice. *International Journal of Rock Mechanics and Mining Science and Geomechanics Abstracts*, *10*(1-2), 1-54. doi: 10.1007/BF01261801

Belem, T., Homand-Etienne, F., & Souley, M. (2000). Quantitative parameters for rock joint surface roughness. *Rock Mechanics and Rock Engineering*, *33*(4), 217-242. doi: 10.1007/s006030070001

Blacic, J. D. (1975). Plastic-deformation on mechanisms in quartz: the effect of water. *Tectonophysics*, *27(3)*, 271-294. doi:10.1016/0040-1951(75)90021-9

Brady, B. H. G., & Brown, E. T. (2006). *Rock mechanics for underground mining*. Netherlands: Springer.

Cai, M. (2008). Influence of intermediate principal stress on rock fracturing and strength near excavation boundaries-insight from numerical modeling. *International Journal of rock Mechanics and Mining Sciences*, *45*, 763-772. doi:10.1016/j.ijrmms.2007.07.026

Colin, D. G., & Paul, R. K. (2012). *IBM SPSS statistics 19 made simple*. New York, NY: Psychology Press.

Colmenares, L. B., & Zoback, M. D. (2002). A statistical evaluation of intact rock failure criteria constrained by polyaxial test data for five different rocks. *International Journal of Rock Mechanics and Mining Sciences*, *39*, 695-729. doi:10.1016/S1365-1609(02)00048-5

Crawford, A. M., & Currant, J. H. (1981). The influence of shear velocity on the frictional resistance of rock discontinuities. *International Journal of Rock Mechanics and Mining Science and Geomechanics Abstracts*, *18*(6), 505-515. doi:10.1016/0148-9062(81)90514-3

Curran, J. H., & Leong, P. K. (1983). Influence of shear velocity on rock joint strength. *Proceeding of International Society for Rock Mechanics and Rock Engineering*, A235-A240.

Fenton, C. H., Charusiri, P., & Wood, S. H. (2003). Recent paleoseismic investigations in Northern and Western Thailand. *Annales Geophysicae*, *46*(5), 957-981. doi: 10.4401/ag-3464

Fuenkajorn, K., & Kenkhuntod, N. (2010). Influence of loading rate on deformability and compressive strength of three Thai sandstones. *Geotechnical and Geological Engineering*, *28*, 707-715. doi:10.1007/s10706-010-9331-7

Fuenkajorn, K., Sriapai, T., & Samsri, P. (2012). Effect of loading rate on strength and deformability of Maha Sarakham salt. *Engineering Geology*, 135-136. doi: 10.1016/j.enggeo.2012.02.012

Haimson, B. (2006). True triaxial stresses and brittle fracture of rock. *Pure and Applied Geophysics*, *163*, 1101-1113. doi:10.1007/s00024-006-0065-7

Haimson, B., & Chang, C. (2000). A new true triaxial cell for testing mechanical properties of rock and its use to determine rock strength and deformability of Westerly granite. *International Journal of Rock Mechanics and Mining Sciences*, *37*(1-2), 285-296. doi:10.1016/S1365-1609(99)00106-9

Haimson, B., & Rudnicki, J. W. (2010). The effect of the intermediate principal stress on fault formation and fault angle in siltstone. *Journal of Structural Geology*, *32*(11), 1701-1711. doi:10.1016/j.jsg.2009.08.017

Jaeger, J. C., Cook, N. G. W., & Zimmerman, R. W. (2007). *Fundamentals of rock mechanics*. Malden, MA: Blackwell Publishing.

Kapang, P., Walsri, C., Sriapai, T., & Fuenkajorn, K. (2013). Shear strengths of sandstone fractures under true triaxial stresses. *Journal of Structural Geology*, *48*, 57-71. doi:10.1016/j.jsg.2012.12.007

Kemthong, R., & Fuenkajorn, K. (2007). Prediction of joint shear strengths of ten rock types using field-identified parameters. *Proceedings of Rock Mechanics*, 195-209.

Kleepmek, M., Khamrat, S., Thongprapa, T., & Fuenkajorn, K. (2016). Displacement velocity effects on rock fracture shear strengths. *Journal of Structural Geology*, *90*, 48-60. doi:10.1016/j.jsg.2016.07.007

Lane, K. S., & Heck, W. J. (1964). Triaxial testing for strength of rock joints. *Proceedings of the 6th U.S. Symposium on Rock Mechanics (USRMS)*, Rolla, Missouri, 98-108.

Li, B., Jiang, Y., & Wang, G. (2012a). Evaluation of shear velocity dependency of rock fractures by using repeated shear tests. *Proceeding of 12th ISRM Congress, Harmonising Rock Engineering and the Environmental*, 699-702.

Li, Y., Wang, J., Jung, W., & Ghassemi, A. (2012b). Mechanical properties of intact rock and fracture in welded tuff from Newberry volcano. *Proceeding of Thirty-seventh Workshop on Geothermal Reservoir Engineering*, Standford University, Standford, California.

Morris, A. P., & Ferrill, D. A. (2009). The importance of the effective intermediate principal stress σ'_2 to fault slip patterns. *Journal of Structural Geology*, *31*(9), 950-959. doi:10.1016/j.jsg.2008.03.013

Odedra, A., Ohnaka, M., Mochizuki, H., & Sammonds, P. (2001). Temperature and pore pressure effects on the shear strength of granite in the brittle-plastic transition regime. *Geophysical Research Letters*, *28*(15), 3011-3014. doi:10.1029/2001GL013321

Ohnaka, M. (1995). A shear failure strength law of rock in the brittle-plastic transition regime. *Geophysical Research Letters*, *22*(1), 25-28. doi:10.1029/94GL02791

Rodklang, K., Khamrat, S., & Fuenkajorn, K. (2015). Effects of temperatures on strength and deformability of Tak granite. *KKU Research Journal*, *20*(3), 272-284.

Rosso, R. S. (1976). A comparison of joint stiffness measurement in direct shear, triaxial compression, and in situ. *International Journal of Rock Mechanics and Mining Sciences and Geomechanics Abstracts*, *13*(6), 167-172. doi:10.1016/0148-9062(76)91282-1

Stesky, R. M. (1978). Rock friction-effect of confining pressure, temperature, and pore pressure. *Pure and Applied Geophysics*, *116*(4), 690-704. doi:10.1007/BF00876532

Yeo, I. W., De Freitas, M. H., & Zimmerman, R. W. (1998). Effect of shear displacement on the aperture and permeability of a rock fracture. *International Journal of Rock Mechanics and Mining Sciences*, *35*(8), 1051-1070. doi:10.1016/S0148-9062(98)00165-X